ACS OMEGA

Open Access



http://pubs.acs.org/journal/acsodf

Article

# Fluorine and Bromine Dual-Doped Nanoporous Carbons: Preparation and Surface Chemistry Studies

Gauhar Mussabek,◆ Saule Baktygerey, Yerzhan Taurbayev, Dana Yermukhamed, Nazym Zhylkybayeva, Vitaliy E. Diyuk, Alexander Zaderko, Sergii Afonin, Ruslan Mariychuk, Mária Kaňuchová, and Vladyslav V. Lisnyak*,◆

Cite This: *ACS Omega* 2024, 9, 38618−38628

Read Online

ACCESS | Metrics & More | Article Recommendations | Supporting Information

**ABSTRACT:** A novel method for the concurrent introduction of fluorine and bromine into the surface of nanoporous activated carbon (NAC) is evaluated. According to the method, the preheated NAC was treated with 1,2-dibromotetrafluoroethane at elevated temperatures (400−800 °C). Potentiometric and elemental analysis, nitrogen adsorption−desorption, scanning electron microscopy-energy-dispersive X-ray spectroscopy, X-ray photoelectron spectroscopy (XPS), and $^{19}$F solid-state NMR were used to study the NAC microstructure and changes in surface chemistry. The specific modification temperature was found to have a decisive influence on the resulting halogen content of the NAC surface. About 1.5 mmol g$^{-1}$ of bromine and only 0.5 mmol g$^{-1}$ of fluorine are chemisorbed on the NAC surface when dual-doped at 400 °C. The fluorination efficiency increases dramatically to 1.84−2.22 mmol g$^{-1}$ when the process temperature is increased to 500−700 °C. Under the same conditions, the bromination efficiency unexpectedly decreases to 0.66−1.32 mmol g$^{-1}$. Since halogen-containing groups undergo significant thermal decomposition around 800 °C, the overall halogenation efficiency decreases, accordingly. Both the volume and surface area of the micropores decrease moderately when halogen-containing groups are introduced into the carbon surface layer. Fluorine and bromine are unevenly distributed in the porous structure of the dual-doped NACs, and the outer surface is more halogen-rich than the inner surface of the micropores. XPS and $^{19}$F solid-state NMR revealed the selective formation of $CF_2$ groups in the NAC surface layer independent of the temperature. In contrast, the percentage of semi-ionic fluorine in the form of CF groups directly bonded to the $\pi$-electron system of the carbon matrix increases significantly with temperature.

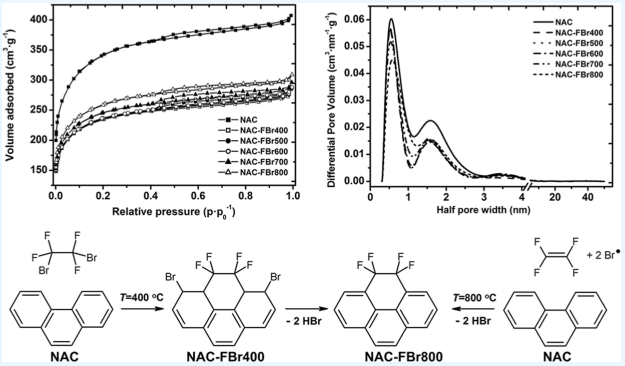


## 1. INTRODUCTION

Fluorine-containing carbon materials have traditionally been widely used in energy storage devices.[1−5] Modifying carbon nanoporous solids with fluorine significantly affects the sorption of water vapor and $CO_2$.[6−8] In many industries, fluorination has a pronounced positive effect on the parameters of amorphous and graphitic carbon solids and carbon nanomaterials.[9−13] Aggressive and toxic reagents such as molecular fluorine, organofluorine compounds, and metal and nonmetal fluorides are commonly used to produce fluorinated carbon materials.[8,9,13−17] Conventional methods are effective and ensure the introduction of a controlled amount of fluorine into the carbon material. However, these methods produce fluorinated materials that are highly enriched in the so-called "semi-ionic" fluorine[18] in the form of C−F bonds. In addition, it is difficult to obtain materials with $CF_2$, $CF_3$, or more complex fluorine-containing surface groups using the currently established methodology.

The presence of two different types of heteroatoms can significantly further modulate the structural, sorption, and chemical properties of carbon materials, which is important for their applications. Dual-doped carbons containing pairs of the following elements: F, S, N, Cl, and/or P, are widely used in electrocatalysis,[19,20] sensors,[21,22] catalysts,[23] as cathodes of lithium/sodium-ion batteries,[24] and supercapacitors.[25]

The primary approach to obtaining such materials is to carbonize materials containing the necessary heteroatoms. This method of obtaining dual-doped carbons ensures a uniform distribution of heteroatoms in the carbon matrix. Importantly, the content of heteroatoms, their ratio, the chemical state of the heteroatoms, and the structural and sorption parameters of the material are determined by the carbonization conditions,

Received: May 1, 2024
Revised: August 7, 2024
Accepted: August 28, 2024
Published: September 5, 2024

providing a level of control over the properties of these materials that cannot be modified separately.

An obvious alternative approach is to produce dual-doped carbons by modifying nanoporous carbon materials. By selecting a specific modifier, certain functional groups can be introduced into the surface layer of the carbon solid. Under controlled modification conditions, the high specific surface area and developed porosity of the starting material are largely retained in the modified product.[4] This expands the application of gaseous haloalkanes and low-molecular-weight organics as fluorinating agents with temperature[26,27] or photochemical activation.[28]

For example, 1,2-dibromotetrafluoroethane (DBTFE), a commercial product formerly known as Freon 114B2 and Halon 2402, is a synthetically useful, readily available, and inexpensive compound for this purpose. It has several potential applications, including fire extinguishers, leak detectors, and refrigerants. Among its many advantages, including non-flammability, active and removable bromine atoms, and a conveniently low boiling point, DBTFE can be used as a useful starting point for the synthesis of fluorinated compounds. These properties have sparked interest in the DBTFE as a reagent in organofluorine chemistry, and Dmowski listed some documented uses for it.[29]

Notably, the Montreal Protocol[30] requires all nations or parties to the protocol to eliminate the production, consumption, and trade of ozone-depleting substances by July 1, 1994. DBTFE has been identified as an ozone-depleting substance due to its high ozone-depleting potential. The use of DBTFE has been restricted and even banned in many countries, except for essential uses or as an analytical standard. As a result, the appropriate use and effective conversion of available DBTFE has become a real challenge because DBTFE can be formed at high temperatures and can be present in the pyrolysis or copyrolysis products of halogenated and halogen-containing plastics or plastics containing brominated flame retardants that need to be dehalogenated.[31−34]

Therefore, this work is devoted to the DBTFE-consuming treatment of nanoporous activated carbon (NAC) sorbent with the gas-phase DBTFE at 400−800 °C, with further focus on the analysis of the changes in surface chemistry after fluorination/bromination.

## 2. MATERIALS AND METHODS

**2.1. Materials.** For the following fluorination/bromination process described below, commercially available Norit granular activated carbon, trade name GAC 830W (Cabot Norit, UK), hereafter referred to as NAC, produced by carbonization and activation of natural coal, was used. To reduce the total ash content, the NAC sorbent was treated with a 5 wt % HCl/HF solution. The resulting deashed NAC was further washed with double-distilled water (DDW) until pH neutralization.

Soft fluorination/bromination of the deashed NAC was performed with DBTFE gas supplied by abcr (Karlsruhe, Germany). The DBTFE was additionally dried by bubbling through concentrated sulfuric acid (Merck, 98%). The use of argon gas (Ar) for inert applications provided an oxygen- and nitrogen-free medium for heat treatment during soft fluorination/bromination. For this purpose, Ar (99.995 vol %) from Linde Gas was used. In this work, acids and other reagents were Merck reagent grade products, which were used as received.

**2.2. Preparation of Dual-Doped NACs.** In a typical fluorination/bromination process, 3 g of deashed NAC was placed in an alundum tube 30 cm long with an inner diameter of 15 mm. This tube, containing the NAC powder, was placed in a horizontal electric tube furnace. The tube's ends were sealed with Viton vacuum flanges (Htc vacuum) with adapters and connected to a vacuum system. The internal volume of the tube was then evacuated by vacuum pumping. The degassed tube was purged with RT Ar gas to remove oxygen and moisture. Subsequently, the furnace was heated from 25 °C to the desired process temperature, which was selected from the range of 400−800 °C with a 100 °C step. Heating to the selected temperature was performed at a rate of 10 °C $min^{-1}$, and the furnace was maintained at this constant temperature by a single-loop proportional-integral-derivative temperature controller (Bajt, KUPP). A gas mixture of DBTFE/Ar (approximately 1:1 by volume) was introduced into the preheated tube containing the NAC powder through a gas supply and a metering system at a total gas velocity of 50 mL $min^{-1}$ for 1 h. The gas supply was then changed to pure Ar, purging the inner volume and the resulting fluorinated/brominated NAC. The furnace was then programmed to cool to an ambient temperature. The fluorinated/brominated NAC, which had been degassed and cooled under an Ar stream, was removed from the tube and transferred to a laboratory glass desiccator containing $CaCl_2$ for drying and storage. The prepared fluorinated/brominated NACs prepared in this manner are hereafter referred to as "NAC-FBrtemperature".

**2.3. Potentiometric Analysis.** The total fluorine [C(F)] and bromine [C(Br)] concentrations in the fluorinated/brominated NACs were determined by potentiometry from the corresponding concentrations of fluoride and bromide ions. For the ion-selective potentiometric analysis, the bound halogens were converted to soluble ionic forms, fluorides and bromides, respectively, by decomposing the carbon solids in the molten mixture of NaOH with a small addition of $NaNO_3$. This conversion was performed in a muffle furnace using the alkali melt stored in a nickel crucible. The resulting melt was dissolved in DDW, and the solution obtained was filtered with a glass funnel filter (Fisherbrand, Sintered Glass Disc filter of grade 3 porosity). The fluoride and bromide contents in the filtered solution were measured using the ELIS-131F fluoride and ELIS-131Br bromide ion-selective electrodes (Izmteh LLC). The signal from the electrodes was recorded in the potentiostat mode using a custom-made potentiometer. This instrument was constructed using an ultraprecision operational amplifier (LMC6001AIM, Texas Instruments).

**2.4. Texture Studies.** Texture studies were performed on a Quantachrome NovaWin2 automatic adsorption analyzer using a standard procedure. Nitrogen ($N_2$) adsorption−desorption isotherms were measured at a liquid $N_2$ temperature. Samples were degassed in situ under vacuum at 160 °C overnight prior to measurements. The specific surface area: $S_{BET}$, $S_{micro}$, $S_{ext}$, $S_{micro}/S_{ext}$ ratio, and the specific volume: $V_{tot}$, $V_{micro}$, and $V_{ext}$ were determined using the instrument software. Pore size distribution (PSD) was determined using the SAIEUS program (Micrometrics Instrument). The isotherm analysis was performed using the Carbon-$N_2$ model for porous carbons with heterogeneous surfaces, derived from two-dimensional nonlocal density functional theory. The bulk density $\gamma$ of the studied dual-doped NACs was determined by the "bottle" method using a Microtrac pycnometer.



https://doi.org/10.1021/acsomega.4c04179
ACS Omega 2024, 9, 38618−38628

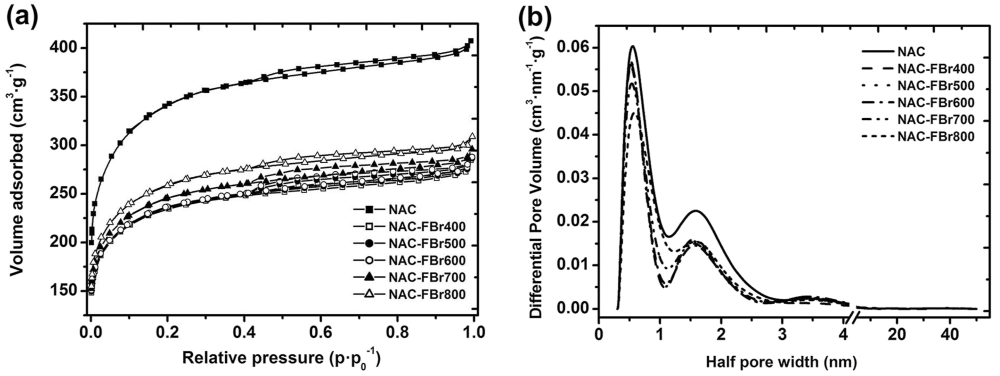


**Figure 1.** (a) $N_2$ adsorption/desorption isotherms and (b) PSD curves for the gas-phase fluorinated/brominated NACs and the unmodified NAC shown in comparison.

**Table 1. Texture Parameters of the Gas-phase Fluorinated/Brominated NACs**

| | | [b]specific surface area ($m^2$ $g^{-1}$) | | | | [c]specific volume ($cm^3$ $g^{-1}$) | | |
|---|---|---|---|---|---|---|---|---|
| samples | [a]$\gamma$ (g $cm^{-3}$) | $S_{BET}$ | $S_{micro}$ | $S_{ext}$ | $S_R$ | $V_{tot}$ | $V_{micro}$ | $V_{ext}$ |
| NAC | 0.433 | 1246 | 1149 | 97 | 11.8 | 0.630 | 0.506 | 0.124 |
| NAC-FBr400 | 0.442 | 855 | 797 | 58 | 13.7 | 0.441 | 0.352 | 0.089 |
| NAC-FBr500 | 0.487 | 859 | 796 | 63 | 12.6 | 0.443 | 0.351 | 0.092 |
| NAC-FBr600 | 0.495 | 862 | 792 | 70 | 11.3 | 0.445 | 0.349 | 0.096 |
| NAC-FBr700 | 0.506 | 894 | 823 | 71 | 11.6 | 0.458 | 0.362 | 0.096 |
| NAC-FBr800 | 0.535 | 942 | 869 | 73 | 11.9 | 0.478 | 0.385 | 0.093 |

[a]$\gamma$ is the bulk density. [b]Specific surface area: $S_{BET}$, $S_{micro}$, $S_{ext}$ are the Brunauer−Emmett−Teller (BET) surface area, micropore surface area, and external surface area, respectively, and $S_R$ is a ratio $S_{micro}/S_{ext}$. [c]Specific volume: $V_{tot}$, $V_{micro}$, $V_{ext}$ are the total specific volume, micropore specific volume, and external pore volume, respectively.

**2.5. Microscopy.** Scanning electron microscopy (SEM) and the energy-dispersive X-ray spectroscopy (EDS) measurements were performed on a Tescan MIRA3 SEM microscope, which was equipped with an Oxford Instruments X-Max 50 silicon drift EDS system with AZtec (Oxford Instruments) and INCA (ETAS) software packages. Samples were dried at 120 °C, cooled, and exposed to vacuum for at least 5 h prior to analysis.

**2.6. X-ray Photoelectron Spectroscopy Analysis.** X-ray photoelectron spectroscopy (XPS) measurements were performed with the SPECSGROUP instrument, which was equipped with a PHOIBOS 100 SCD analyzer and a nonmonochromatic X-ray source. The survey surface spectrum was acquired at a transition energy of 70 eV, while the core spectra were obtained at 30 eV at ambient temperature. All spectra were recorded at a base pressure of $2 \times 10^{-8}$ mbar with Al K$\alpha$ excitation at 10 kV (150 W). The data were analyzed using SpecsLab2 software (Casa Software). The Shirley and Tougaard baselines were used for all peak fits. All samples studied exhibited varying degrees of charging due to their partial insulating nature. The spectrometer was calibrated against carbon (C 1s).

**2.7. $^{19}$F Solid State Nuclear Magnetic Resonance ($^{19}$F ssNMR) Measurements.** To evaluate the identity of the fluorine-containing functional groups, $^{19}$F ssNMR measurements were performed using a wide-bore (Bruker Avance III) spectrometer operating at 470 MHz for $^{19}$F. The powders were filed into 2.5 mm outer diameter rotors (Bruker) and measured at 22 kHz spinning under magic angle, employing a Bruker triple resonance HFX MAS probe. Samples were measured at 40 °C. 1-Pulse experiments with a 90 pulse width of 2.4 $\mu$s with or without 25 kHz TPPM $^1$H decoupling and 5 s recycle time were used to acquire the $^{19}$F ssNMR spectra, referenced to the $CFCl_3$ peak at 0.0 ppm.

## 3. RESULTS AND DISCUSSION

**3.1. Texture Studies.** The $N_2$ adsorption isotherms for the unmodified (starting) NAC and the fluorinated/brominated NACs (Figure 1a) correspond to those of nanoporous solids, as evidenced by the significant $N_2$ adsorption at low pressures. As can be seen from Table 1, the modification leads to a decrease in the adsorption capacity, albeit moderate, compared to the unmodified NAC. For the fluorinated/brominated NACs, the values of Brunauer−Emmett−Teller surface area ($S_{BET}$) and total specific volume ($V_{tot}$) are estimated to be about 70−75% of the corresponding values for the unmodified NAC (Table 1). The lowest values of $S_{BET}$ and $V_{tot}$ are observed for the NAC-FBr400, and as the modification temperature is increased, the texture parameters increase slightly. The surface area of the micropores ($S_{micro}$) is the main contributor to the $S_{BET}$ for all the nanoporous solids studied (cf. $S_{micro}$ and $S_{BET}$ in Table 1). The recorded isotherms have narrow hysteresis loops, indicating the presence of mesopores in the bulk of the nanoporous solids. After fluorination/bromination, the contribution of the mesopore surface area ($S_{ext}$) to the total surface area remains relatively modest, with values ranging from 7 to 9% of the $S_{BET}$ (Table 1).

The PSD curves (Figure 1b) show that the porous structure of unmodified NAC and fluorinated/brominated NACs is almost entirely represented by micropores. Two different types of micropores can be identified within the porous structure. The first type has an average size of 0.53−0.58 nm, while the second type has an average size of 1.6 nm. As the fluorination/bromination temperature increases, the number of micropores


https://doi.org/10.1021/acsomega.4c04179
ACS Omega 2024, 9, 38618−38628

belonging to the above types decreases, and no rearrangement of pore width is observed. As shown in Figure 1b, the PSD curves indicate the presence of a small number of mesopores with an approximate width of 3.3−3.6 nm. The number of these mesopores increases with increasing modification temperature.

Consequently, the fluorinated/brominated NACs exhibit analogous shape isotherms and thus analogous structural and sorption properties. It is noteworthy that the fluorinated/brominated NACs prepared at medium−high temperatures, below and at 600 °C, exhibit remarkably similar texture parameters (Table 1). This observation suggests that a similar modification mechanism may be at work. As a consequence of the modification, a significant increase in the bulk density $\gamma$ is observed. The most likely explanation for this phenomenon is the formation of a layer of halogen-containing groups on the carbon surface, filling the smallest micropores (Table 1).

**3.2. SEM Imaging, EDS, XPS and Potentiometric Analyses.** The macrostructure of the top surface and elemental composition of the modified NACs were investigated using SEM and the EDS method. Figure 2 illustrates the SEM images characterizing the surface relief for the unmodified NAC compared with an example of a fluorinated/brominated NAC.

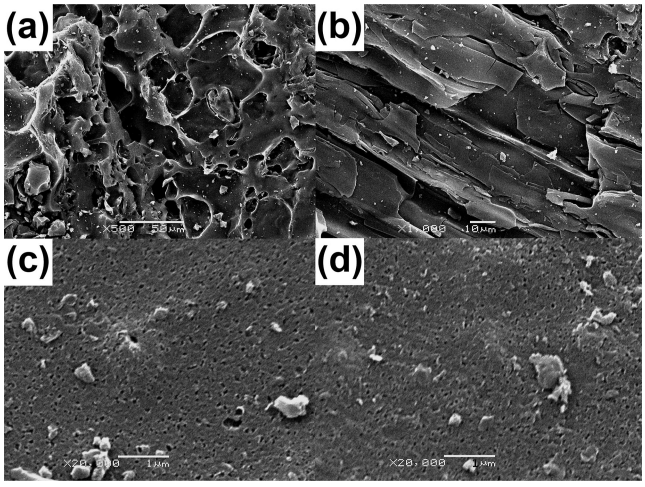


**Figure 2.** Representative SEM images of the initial and modified NACs: (a) NAC × 500, (b) NAC × 1000, (c) NAC × 20,000, and (d) NAC-FBr600 × 20,000.

The unmodified NAC is characterized by a considerable number of large voids and channels, with the channels measuring up to 20−30 $\mu$m in width. The inner surfaces of these channels exhibit a relatively smooth texture (Figure 2a). Additionally, there are areas of layered regular structures (Figure 2b). These structural elements are the structural remnants of the coal used to prepare the NAC and are considerably larger than the macropores.

Fluorination/bromination does not alter the macrostructure. In the macrostructure of the unmodified NAC, significant areas with a regular distribution of tiny pores, smaller than 100 nm, can be identified (Figure 2c,d). These pores, however, are attributed to macropores or large mesopores, and their distribution is not significantly altered by fluorination/bromination.

Table 2 presents a summary of the potentiometric analysis for fluoride and bromide, along with the elemental composition data obtained by the EDS and XPS for the fluorinated/brominated NACs. The results of the potentiometric analysis indicate that the modification of NAC with DBTFE is an effective method for the simultaneous introduction of fluorine (fluorine-containing groups) and bromine (bromine-containing groups) into the carbon surface layer. However, the fluorine and bromine contents in the dual-doped NACs are significantly affected by the processing temperature. The fluorine concentration in the NAC-FBr400 is only 0.5 mmol $g^{-1}$. As the modification temperature increases, the fluorine content also increases significantly. The maximum concentration of fluorine (2.22 mmol $g^{-1}$) is found in the NAC-FBr700. However, when the modification temperature is further increased to 800 °C, the fluorine content begins to decrease due to the significant thermolysis of chemisorbed fluorine, its reaction with surface hydrogen, and the subsequent thermodesorption in the form of HF.

Notably, the bromine content in the dual-doped NACs reaches its maximum for the NAC-FBr400. However, as the modification temperature increases, the bromine content experiences a significant decrease. This contrast in the temperature dependence of the fluorine and bromine contents results in very different concentration $C(F)/C(Br)$ ratios. For example, the bromine content in NAC-FBr400 is about three times higher than the fluorine content. In NAC-FBr700, however, the fluorine content exceeds the bromine content by a factor of 3.4, highlighting the dynamic nature of the modification process and the influence of temperature on the elemental composition.

The EDS and XPS data show similar temperature dependencies for the fluorine and bromine contents. Moreover, the surface layer (XPS data) is significantly enriched in halogens, with their content on the surface being 2.6−3.1 times higher than in the volume of the bulk solid (EDS data). A negative correlation between the oxygen and halogen contents suggests the involvement of oxygen-containing groups in the fluorination/bromination process.

**Table 2. Results of Potentiometric and Elemental Analyses of the Gas-phase Fluorinated/Brominated NACs**

| | potentiometry | | | EDS | | | | XPS | | | |
|---|---|---|---|---|---|---|---|---|---|---|---|
| | concentration (mmol $g^{-1}$) | | | elemental content (wt %) | | | | elemental content (wt %) | | | |
| sample | C(F) | C(Br) | C(F)/C(Br) | C | O | F | Br | C | O | F | Br |
| NAC | 0 | 0 | | 94.3 | 5.7 | | | 89.8 | 10.2 | | |
| NAC-FBr400 | 0.50 | 1.49 | 0.34 | 81.8 | 4.8 | 1.1 | 12.3 | 55.1 | 4.1 | 3.1 | 37.7 |
| NAC-FBr500 | 1.84 | 1.32 | 1.39 | 82.0 | 3.5 | 3.8 | 10.7 | 57.1 | 3.3 | 10.0 | 29.6 |
| NAC-FBr600 | 2.05 | 0.84 | 2.44 | 85.8 | 3.1 | 4.1 | 7.0 | 67.0 | 3.1 | 12.4 | 17.5 |
| NAC-FBr700 | 2.22 | 0.66 | 3.36 | 86.5 | 3.5 | 4.5 | 5.5 | 68.4 | 3.9 | 13.8 | 13.9 |
| NAC-FBr800 | 1.55 | 0.60 | 2.58 | 87.2 | 4.6 | 3.2 | 5.0 | 72.4 | 5.7 | 9.2 | 12.7 |



https://doi.org/10.1021/acsomega.4c04179
ACS Omega 2024, 9, 38618−38628

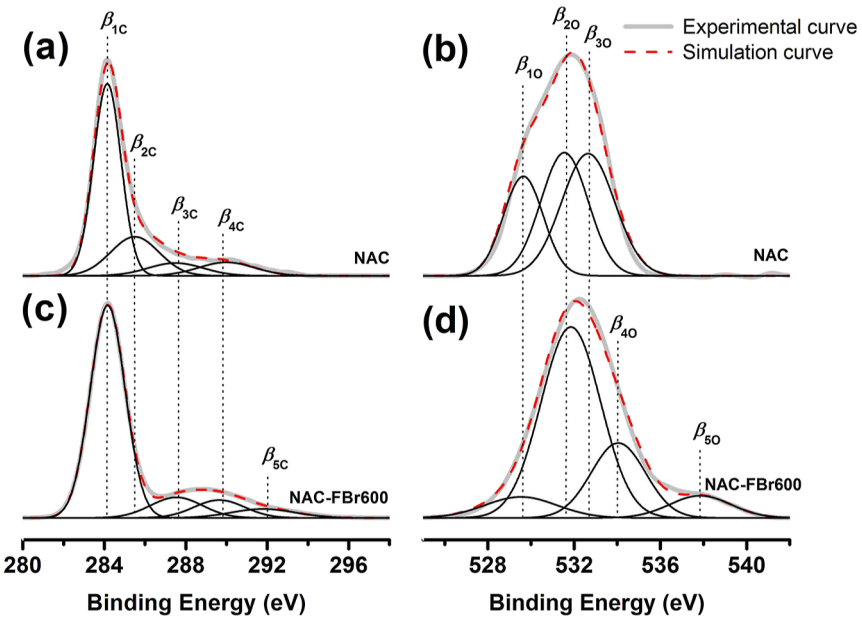


**Figure 3.** Representative (a,c) C 1s and (b,d) O 1s core levels XP spectra for (a,b) NAC (c,d) NAC-FBr600.

The results of SEM-EDS elemental mapping of the NAC-FBr400 and NAC-FBr600 are shown in Figures S1 and S2 (Supporting Information). As can be seen, the identified elements C, O, F, and Br, which are the main components of the samples, are generally uniformly distributed. By the EDS mapping, it was obtained analogous elemental distribution images for NAC-FBr400 ($C(F)/C(Br)$ = 0.34) and NAC-FBr600 ($C(F)/C(Br)$ = 2.44). This fact again confirms the chemical modification of the NAC surface when interacting with DBTFE at different temperatures. Areas of slightly higher intensity (higher element content) probably correspond to different nanopores (micropores and mesopores), while the empty (black) areas correspond to transport channels and large macropores in the solid carbon matrix. Higher chemisorption of O, F, and Br heteroatoms can be observed in nanopores on a heterogeneous carbon surface. Comparing the EDX mapping of O, F, and Br with each other (see Figures S1c−e and S2c−e), some differences in the distribution of these elements can be observed, namely: (i) the differences between the distribution of O on the one hand and F and Br on the other hand indicate the competition between these elements for the active centers of the surface of NAC. The removal of oxygen (oxygen-containing groups) during heating frees active centers for chemisorption of F and Br; (ii) the differences in the distribution of F and Br indicate the independent interaction of these two elements with the active centers of the surface of NAC. The rational reasons for these observations are the thermal decomposition of DBTFE molecules with the formation of atomic and molecular bromine and, in addition, the different diffusion capacities of the thermal decomposition products of DBTFE molecules pyrolyzed in the porous structure of NAC. This result is consistent with those described and discussed earlier by comparing EDS and XPS data (Table 2).

It is reasonable to assume that halogen-containing groups will occupy the surface centers that are formed by the decomposition or thermal decomposition of oxygen-containing groups. In addition, decomposition products of oxygen-containing groups may participate in the partial pyrolysis of DBTFE. The resulting reactive intermediates are chemisorbed to the surface carbon centers. A slight increase in the surface oxygen concentration for the NAC-FBr800 can be attributed to the formation of new oxygen-containing groups on the carbon surface due to the "aging" of the sample. This latter process is accompanied by the hydrolysis of the most unstable forms of added fluorine and bromine and the oxidation of surface defects formed as a result of thermodesorption processes at high temperatures. Thus, our results indicate that the modification of NAC involves the partial pyrolysis of DBTFE with the formation of various intermediates. Bromine-containing intermediates show higher reactivity at low temperatures while fluorine-containing intermediates are most reactive at 700 °C. The low bromine content at high temperatures can be explained by the lower bond dissociation energy for C−Br bonds (275 kJ $mol^{-1}$) compared to C−F bonds (485 kJ $mol^{-1}$), providing a qualitative understanding of the inherent complexity of the modification process.

**3.3. Core Level XP Spectra Analysis.** Figure 3 shows the typical C 1s (Figure 3a,c) and O 1s (Figure 3b,d) core level XP spectra of the fluorinated/brominated NACs.

The experimental data for the C 1s core level XP spectra were fitted with four to five curves with a full width at half-maximum of 1.5−2.5 eV (Figure 3a), taking into account the structure of the functional groups on the surface of the activated carbon.[35,36] This approach allowed for the identification of the specific functional groups present on the surface of the activated carbon. The resulting fit of the C 1s core level XP spectrum for the unmodified NAC (Table 3) indicates the presence of four components, designated as $\beta_{1C}$, $\beta_{2C}$, $\beta_{3C}$, and $\beta_{4C}$. These components can be attributed to specific binding energies corresponding to the following bonds: the C═C conjugated bonds, C−O bonds belonging to phenolic groups, C═O bonds (quinone surface groups), and O−C═O bonds belonging to carboxyl, anhydride, and lactone groups, respectively. Among the various oxygen-containing functional groups, phenolic groups, the assigned component $\beta_{2C}$, have the highest concentration of 21.8% on the NAC surface (Table 3).


https://doi.org/10.1021/acsomega.4c04179
ACS Omega 2024, 9, 38618−38628

Table 3. XP Spectra Analysis of the C 1s and O 1s Core Levels in the Selected Gas-phase Fluorinated/Brominated NACs

| | C 1s | | | | | O 1s | | | |
|---|---|---|---|---|---|---|---|---|---|
| | binding energy (eV); and content (%) | | | | | | | | |
| sample | $\beta_{1C}$ C−C | $\beta_{2C}$ C−O | $\beta_{3C}$ C=O, C−Hal | $\beta_{4C}$ O−C=O, CF−($CF_x$) | $\beta_{5C}$ $CF_2$ | $\beta_{1O}$ O−C=O | $\beta_{2O}$ (C=O) | $\beta_{3O}$ (C−O) | $\beta_{4O}$ C−O (Hal) | $\beta_{5O}$ C−O ($CF_2$) |
| NAC | 284.2 (61.4) | 285.5 (21.8) | 287.5 (8.1) | 290.0 (8.7) | | 529.6 (24.3) | 531.6 (35.9) | 532.7 (39.8) | | |
| NAC-FBr400 | 284.2 (74.6) | | 287.6 (14.1) | 289.8 (8.1) | 292.1 (3.2) | 529.5 (11.1) | 531.8 (59.0) | | 534.2 (25.3) | 538.0 (4.6) |
| NAC-FBr600 | 284.2 (75.4) | | 287.6 (10.7) | 289.8 (9.1) | 292.0 (5.8) | 529.5 (8.2) | 531.8 (62.1) | | 534.1 (22.1) | 537.9 (7.4) |
| NAC-FBr800 | 284.2 (78.5) | | 287.6 (4.6) | 289.8 (12.2) | 292.1 (4.7) | 529.6 (20.8) | 531.8 (57.0) | | 534.1 (17.3) | 537.8 (4.8) |

In the high-resolution C 1s core level XP spectra (Figure 3c), the $-CF_2$ (291.2−292.2 eV) and C−C (284.2−284.6 eV) peaks are easily identified.[37] After fluorination, there is no sign of the $-CF_3$ (293.7−294.2 eV[37−39]) signal in the C 1s core level XP spectra. Fluorination/bromination of the NAC results in significant changes in the C 1s core level XP spectrum. For example, the $\beta_{2C}$ component disappears almost completely, while a new $\beta_{5C}$ component appears, indicating the presence of $CF_2$ groups (Figure 3c). The fraction of carbon involved in the formation of $CF_2$ groups in the fluorinated/brominated NACs is consistent with the added fluorine content. The contributions of the other components show some variability. A notable decrease in the $\beta_{4C}$ component is attributed to the elimination of carboxyl, anhydride, and lactone groups during heating. A slight increase in the $\beta_{3C}$ component is discernible due to an increase in the relative content of C=O groups, the contribution of C−Hal bonds, and that of the C−O bonds adjacent to Hal-containing groups. These changes are corroborated by the O 1s core level XP spectrum (Figure 3b,d). A significant decrease in the content of the $\beta_{1O}$ component and a slight increase in the $\beta_{2O}$ component are observed, consistent with the pronounced thermal stability of the oxygen-containing functional groups. In the case of the fluorinated/brominated NACs, the $\beta_{3O}$ component is absent in the XP spectrum of the O 1s core level, while two new components, $\beta_{4O}$ and $\beta_{5O}$, appear. These components are attributed to the C−O bonds in phenolic groups located adjacent to the incorporated bromine atoms and fluorine-containing groups, respectively.

Figure 4 depicts the core-level F 1s and Br 3d XP spectra of the fluorinated/brominated NACs.

In general, F 1s spectra are only deconvolved into the components assigned to covalent, semi-ionic, and ionic bonds.[18,40,41] The F 1s peaks of ionic bonds at ∼684 eV are not observed in the spectra (Figure 4a). The F 1s peaks of covalent and semi-ionic C−F bonds are located at 688.3 eV and 685.9 ± 0.1 eV, respectively. Based on their binding energies, it can be postulated that during the gas-phase modification, the covalent C−F bonds are partially converted into semi-ionic C−F bonds, which provides a reasonable explanation for the lower content of F moieties. The XP spectral data obtained at the F 1s core level for the NAC-FBr400 and NAC-FBr600 can be satisfactorily described with only two components (Figure 4a).

No forms with a binding energy of 689.6 eV[42] that could be attributed to the $CF_3$ group, were identified in these spectra. The majority of the chemisorbed fluorine (more than 70−80%) in the NAC-FBr400 and NAC-FBr600 is in the form of $CF_2$ groups ($\beta_{3F}$), while the other form ($\beta_{1F}$) corresponds to a variety of fluorine-containing groups with semi-ionic $C-F_{SI}$ bonds (Table 4). The semi-ionic type of bonding implies a direct interaction between the chemisorbed fluorine and the conjugated (aromatic) system of C=C bonds of the carbon matrix. This type of bonding is typical of fluorinated graphitic carbons and other carbon nanomaterials.[18,43−45]

In the case of the NAC-FBr800, three spectral components are required to deconvolve the F 1s core level XP spectrum. The $\beta_{2F}$ component corresponds to the energy of the C−F bonds that can be formed as a result of thermochemical transformations of DBTFE at high temperatures. Consequently, as the fluorination/bromination temperature increases, an increase in the contribution of $C-F_{SI}$ semi-ionic groups is documented, and the appearance of a new form of


https://doi.org/10.1021/acsomega.4c04179
ACS Omega 2024, 9, 38618−38628

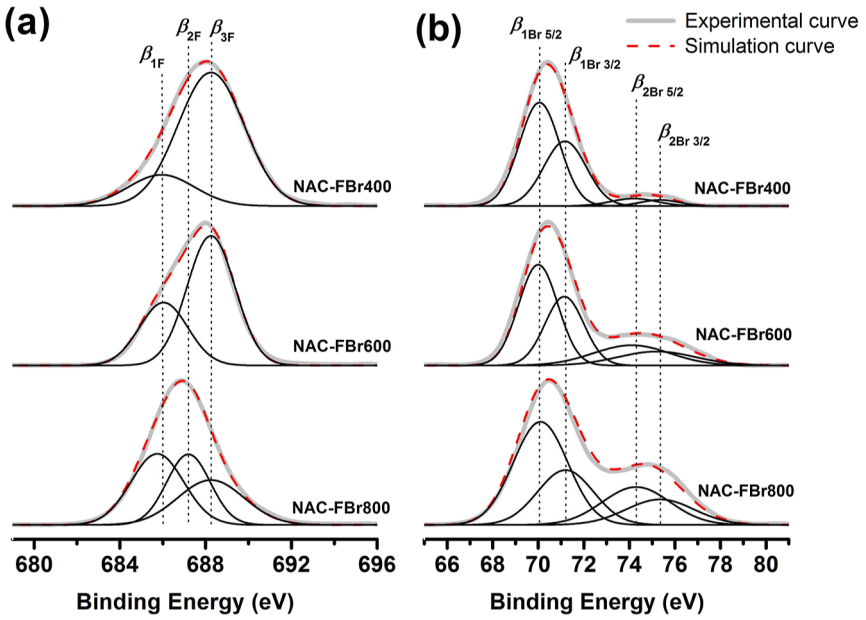


**Figure 4.** Representative (a) F 1s and (b) Br $3d_{5/2}$ core levels XP spectra for the gas-phase fluorinated/brominated NACs.

**Table 4. XP Spectra Analysis of the F 1s and Br $3d_{5/2}$ Core Levels of Selected Gas-phase Fluorinated/Brominated NACs**

| | $E_b$, eV; and content (%) | | | | |
|---|---|---|---|---|---|
| | F 1s | | | Br $3d_{5/2}$ | |
| sample | $\beta_{1F}$C−$F_{SI}$ | $\beta_{2F}$C−F | $\beta_{3F}CF_2$ | $\beta_{1Br}$C−Br | $\beta_{2Br}$C−Br (F, O) |
| NAC-FBr400 | 685.9 (19.0) | | 688.3 (81.0) | 70.1 (92.4) | 74.2 (7.6) |
| NAC-FBr600 | 686.0 (28.3) | | 688.3 (71.7) | 70.0 (71.6) | 74.1 (28.4) |
| NAC-FBr800 | 685.8 (38.4) | 687.1 (31.3) | 688.3 (30.3) | 70.1 (68.7) | 74.3 (31.3) |

$\beta_{2F}$ (C−F bonds) is attributed to a decrease in the contribution of $CF_2$ covalent bonds (Table 4).

Two forms of chemisorbed bromine can be distinguished in the Br 3d core level XP spectra for the fluorinated/brominated NACs (Figure 4b). These forms can be fitted with two peaks, taking into account the spin−orbit splitting of the signal into Br $3d_{5/2}$ and Br $3d_{3/2}$ components. It is known that the Br $3d_{5/2}$ and Br $3d_{3/2}$ components have a difference in energy of about 1.05 eV and intensity, which are correlated as 3:2. Table 3 shows the binding energy and the total area of the two peaks fitted to the Br $3d_{5/2}$ signal, which is the most intense of the pair. The lower binding energy $\beta_{1Br}$ component, which is the most intense, corresponds, by binding energy, to "single" C−Br bonds that are relatively distant from other halogen-containing groups. The contribution of this component to the Br $3d_{5/2}$ signal is in the range of 68−92%, with the contribution of the component decreasing with increasing treatment temperature. The higher binding energy component ($\beta_{2Br}$) is attributed to the C−Br bonds directly interacting with fluorine (oxygen) atoms. As the fluorination/bromination temperature increases from 400 to 800 °C, the contribution of such C−Br bonds to the $\beta_{2Br}$ component increases by more than 4-fold. Consequently, an increase in the fluorination/bromination temperature results in the formation of surface forms of halogens that interact more with the carbon matrix (forming semi-ionic fluorine) and with each other.

**3.4. $^{19}$F ssNMR Spectra Analysis.** In the analysis of the $^{19}$F ssNMR spectra of the fluorinated/brominated NACs (Figure 5), we used the following chemical shift (CS) ranges to assign fluorine-containing groups: The isotropic signals of $CF_3$ groups are expected to occupy a range of 0 to −80 ppm, those of $CF_2$ groups, a range of −50 to −130 ppm, those of aromatic fluorine (Ar−F) groups, a range of −100 to −200 ppm, and those of CF groups, a range of −120 to −280 ppm.[46−48]

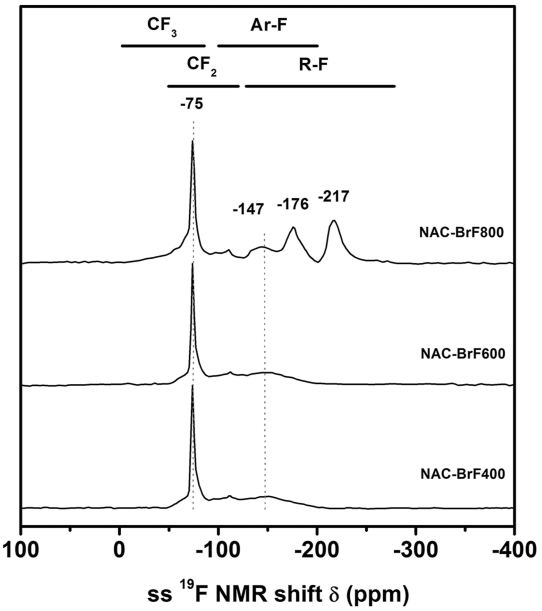


**Figure 5.** Representative $^{19}$F ssNMR spectra of the fluorinated/brominated NACs.

According to Panich,[49] in the fluorinated carbon nanomaterials, the signal in the CS region between −50 and −120 ppm



https://doi.org/10.1021/acsomega.4c04179
ACS Omega 2024, 9, 38618−38628

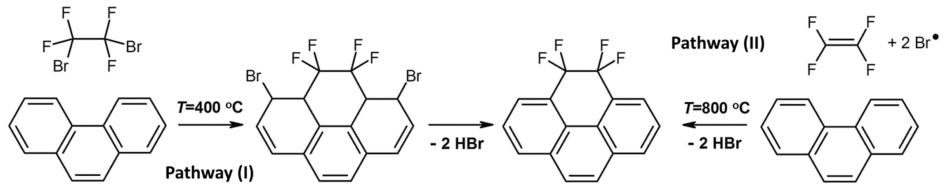


**Figure 6.** Scheme of the NAC carbon surface fluorination and bromination with 1,2-dibromotetrafluoroethane. It illustrates two possible pathways: a low-temperature, ionic mechanism-based process (I) on the left and a high-temperature, radical-based process (II) on the right.

may originate from both the $CF_2$ and $CF_3$ groups resulting from the fluorination of the edges of the carbon planes.

According to Figure 5, the $^{19}F$ ssNMR spectra show a very intense peak at −75 ppm. This signal, considering the structure of DBTFE as the NAC modifier, can be attributed to the $CF_2$ groups, rather than the $CF_3$ groups, as the latter were not present in the studied materials according to other methods (see above). In addition to this resonance, the spectra of NAC-FBr400 and NAC-FBr600 show very low intensity signals between −130 and −180 ppm. These signals can be attributed to the CF groups, as proposed by Hagaman et al.[48] These monofluoro-CF groups are likely to be the "semi-ionic" forms of the chemisorbed fluorine. It is plausible that these groups are present in both aromatic and aliphatic (R−F) moieties. The low intensity of these signals is consistent with the XPS data.

The $^{19}F$ ssNMR spectrum of the NAC-FBr800 (Figure 5) shows the appearance of several novel resonances that can be attributed to CF groups with different characteristics of C−F bonds. The formation of these surface forms of fluorine is possible due to chemisorption of DBTFE pyrolysis products on the carbon surface (here DBTFE pyrolysis occurred at elevated temperatures) or due to thermal decomposition processes in the carbon surface layer. The broadened peaks at −210 and −176 ppm correspond to the fluorine atoms forming covalent bonds with aliphatic and aromatic fragments of the carbon matrix, respectively. This is consistent with the general rule that the lower the CS, the higher the covalency.[47] The formation of the aliphatic fragments of the carbon matrix is associated with the partial destruction of the aromatic conjugated system and the heterogenization of the carbon surface layer under the influence of high temperatures and the action of pyrolysis products of DBTFE.

The covalence of a bond increases as the CS decreases. This relationship is particularly relevant for CF groups, which can form semi-ionic bonds. These CF groups may be responsible for the low intensity broad peak at −147 ppm. Another factor contributing to this signal is the presence of "linked" CF groups, which can be found in various forms such as midchain, cyclic, or branched groups. These "linked" CF groups are characterized by having at least two fluorinated carbon atoms attached to them.[50]

The formation of fluorine-containing groups on carbon surfaces is contingent upon temperature. To comprehend the temperature dependence, it is essential to conceptualize the potential chemical reactions involving DBTFE in the presence of a carbon surface and to discretize the diverse range of surface products that could potentially be generated following the partial decomposition of DBTFE when decomposition products react with NAC surface. The most straightforward process achievable at any temperature under investigation results in the formation of radicals ($Br^•$ and $BrF_2C-^•CF_2$) and tetrafluoroethylene, $F_2C{=}CF_2$.[51] It is also possible that some parallel processes involving the carbon surface layer may occur during thermolysis, resulting in the generation of byproducts (see the Supporting Information, Texts S1 and S2 and additional refs 52−61).

As the reaction temperature increases, the number of DBTFE molecules undergoing deep pyrolysis also increases. The partial decomposition of DBTFE can be illustrated by the following equation

$$BrF_2C-CF_2Br \leftrightarrow BrF_2C-^•CF_2 + Br^• \leftrightarrow F_2C{=}CF_2 + 2Br^•(Br_2)$$

Bromine radicals, or dibromine molecules, can engage in various substitution and addition reactions with the C=C bonds of the carbon matrix. Bromine addition is selective and independent of the fluorine addition, as demonstrated by the results of the chemical analysis. The temperature dependence of the amount of chemisorbed bromine is in good agreement with the proposed pyrolysis mechanism. It is noteworthy that the observed decrease in the surface bromine concentration at temperatures of 600−700 °C can be explained by the low bond dissociation energy for C−Br (275 kJ $mol^{-1}$).

The introduction of fluorine into the NAC carbon surface, predominantly in the form of $CF_2$ groups, is possible via two different pathways. The first pathway (I), which follows a purely ionic mechanism, involves the addition of the entire DBTFE molecule to a complex active center consisting of two adjacent HC=CH bonds on the carbon surface (Figure 6).

This addition creates an intermediate in which a cyclized $CF_2-CF_2$ group is formed, and the adjacent carbon atoms become brominated due to proximity-induced structural rearrangement. Restoration of the conjugated carbon bond system in the carbon matrix and the formation of a stable cyclization product can be readily achieved by eliminating two HBr molecules by heating. While this pathway is limited by a relatively small number of active centers, it is particularly effective at temperatures above 400 °C. The second pathway, the radical-based process (II) shown in Figure 6, which also leads to the formation of the same product, involves the products of the DBTFE pyrolysis, specifically, $BrF_2C-^•CF_2$ or $F_2C{=}CF_2$. This addition reaction is favored at elevated temperatures, and proceeds by a radical mechanism. At temperatures in the range of 600−800 °C, a sufficient amount of active products are generated in the gaseous reaction mixture due to the pyrolysis of DBTFE. In addition, the carbon matrix itself is further activated by the thermal decomposition of the oxygen-containing groups.[62] Consequently, the reactions of $BrF_2C-^•CF_2$ or $F_2C{=}CF_2$ with the carbon matrix should result in the formation of the $CF_2$ surface groups with high selectivity, as shown in Figure 6.

The partial pyrolysis of DBTFE is consistent with the hypothesis that the $^{19}F$ ssNMR signal at −75 ppm should be attributed to $CF_2$ groups rather than $CF_3$ groups (Figure 5). The formation of $CF_3$ groups requires a more profound pyrolysis of DBTFE, involving the cleavage of C−C and C−F


https://doi.org/10.1021/acsomega.4c04179
ACS Omega 2024, 9, 38618−38628

bonds and subsequent rearrangement. Such a process can only occur at high temperatures and it is evident that it cannot ensure the selective formation of the same functional groups in large quantities over the tested temperature range.

## 4. CONCLUSIONS

A commercial NAC has been successfully fluorinated and brominated (dual-doped) in the gas phase by a simple technique. The fluorination/bromination of NAC at 400 °C results in the chemisorption of about 1.5 mmol $g^{-1}$ of bromine and only 0.5 mmol $g^{-1}$ of fluorine. The low fluorine content in the low temperature treated NAC can be attributed to the low abundance of active centers capable of binding the entire DBTFE molecule, as well as the inactivity of the DBTFE pyrolysis products at low temperatures. In addition, competition for surface active centers between fluorine-containing molecules and bromine radicals (dibromine molecules) is another contributing factor.

By increasing the temperature of the NAC modification process to a range of 500−700 °C, it has been observed that the efficiency of fluorine grafting is significantly increased, resulting in the formation of $CF_2$ groups. This phenomenon can be attributed to two main factors: (i) enhanced partial pyrolysis of DBTFE to form $BrF_2C-{}^{\bullet}CF_2$ or $F_2C{=}CF_2$; and (ii) additional surface activation due to thermal destruction of various, including bromine-containing, functional groups. As the halogenation temperature is further increased to 800 °C, the efficiency of the halogen chemisorption decreases slightly due to the increasing contribution of the thermal decomposition of the grafted groups. The process becomes nonselective due to the significant pyrolysis of DBTFE and the involvement of various active centers of the NAC surface in the gas-phase modification. The $^{19}F$ ssNMR showed that the added fluorine is mainly in the form of $CF_2$ groups, regardless of the modification temperature.

The modification temperature is a key factor, and its variation allows a controlled preparation of dual-doped nanoporous carbon solids whose surface layers are selectively enriched with either fluorine or bromine. The fluorination/bromination process studied has been shown to be mild, since it does not lead to significant changes in the macro- and microstructure (overall porosity) of NAC, as evidenced by SEM and $N_2$ adsorption−desorption results. The introduction of halogen-containing groups, independent of the temperature, only moderately decreased of the surface area and micropore volume. At the same time, fluorine and bromine are unevenly distributed in the porous structure of NAC, with the outer surface of NAC being enriched with halogens relative to the inner surface of the micropores.

The modification of NAC with DBTFE in the gas phase is a convenient and efficient method for the selective preparation of F- and Br-containing dual-doped nanoporous carbons for various modern applications and DBTFE conversion.

## ■ ASSOCIATED CONTENT

### Supporting Information

The Supporting Information is available free of charge at https://pubs.acs.org/doi/10.1021/acsomega.4c04179.

Figures S1 and S2: Representative SEM micrographs and EDS elemental mappings of the NAC-FBr400 and NAC-FBr600. Text S1 presents the results of analytical tests and ion-selective potentiometry data. Text S2 summarizes some possible thermolysis products taken from the literature data[52−61] (PDF)

## ■ AUTHOR INFORMATION


### Corresponding Author

**Vladyslav V. Lisnyak** − *Nanotechnological Laboratory of Open Type, Al-Farabi Kazakh National University, 050040 Almaty, Kazakhstan; Faculty of Chemistry, Taras Shevchenko National University of Kyiv, 01601 Kyiv, Ukraine; Western Caspian University, AZ 1001 Baku, Republic of Azerbaijan; Institute of Macromolecular Chemistry, The National Academy of Sciences of Ukraine, 02160 Kyiv, Ukraine;* orcid.org/0000-0002-6820-1445; Email: lisnyak@univ.kiev.ua

### Authors

**Gauhar Mussabek** − *Nanotechnological Laboratory of Open Type, Al-Farabi Kazakh National University, 050040 Almaty, Kazakhstan; Institute of Information and Computational Technologies, 050012 Almaty, Kazakhstan*

**Saule Baktygerey** − *Nanotechnological Laboratory of Open Type, Al-Farabi Kazakh National University, 050040 Almaty, Kazakhstan; Institute of Information and Computational Technologies, 050012 Almaty, Kazakhstan*

**Yerzhan Taurbayev** − *Nanotechnological Laboratory of Open Type, Al-Farabi Kazakh National University, 050040 Almaty, Kazakhstan*

**Dana Yermukhamed** − *Nanotechnological Laboratory of Open Type, Al-Farabi Kazakh National University, 050040 Almaty, Kazakhstan; Institute of Information and Computational Technologies, 050012 Almaty, Kazakhstan*

**Nazym Zhylkybayeva** − *Nanotechnological Laboratory of Open Type, Al-Farabi Kazakh National University, 050040 Almaty, Kazakhstan; Institute of Information and Computational Technologies, 050012 Almaty, Kazakhstan*

**Vitaliy E. Diyuk** − *Faculty of Chemistry, Taras Shevchenko National University of Kyiv, 01601 Kyiv, Ukraine*

**Alexander Zaderko** − *Light Matter Institute, UMR-5306, Claude Bernard University of Lyon/CNRS, Université de Lyon, 69622 Villeurbanne Cedex, France*

**Sergii Afonin** − *Institute of Biological Interfaces (IBG-2), Karlsruhe Institute of Technology, 76021 Karlsruhe, Germany*

**Ruslan Mariychuk** − *Department of Ecology, Faculty of Humanities and Natural Sciences, University of Prešov in Prešov, 08001 Prešov, Slovakia*

**Mária Kaňuchová** − *Institute of Earth Resources, Faculty of Mining, Ecology, Process Control and Geotechnology, Technical University of Košice, 042 00 Košice, Slovakia*

Complete contact information is available at: https://pubs.acs.org/10.1021/acsomega.4c04179

### Author Contributions

♦G.M. and V.V.L. contributed equally.


### Notes

The authors declare no competing financial interest.

## ■ ACKNOWLEDGMENTS

This research was funded by the Committee of Science of the Ministry of Science and Higher Education of the Republic of Kazakhstan, grant no. BR21882187. V.V.L. acknowledges the partial support of the Ministry of Education and Science of

Ukraine under grant 0122U002023 and the support of the National Research Foundation of Ukraine (NRFU), the NRFU grant 2023-3-193. This work was supported in part by the Ministry of Education and Science of Ukraine: grant of the Ministry of Education and Science of Ukraine for perspective development of a scientific direction: "Mathematical Sciences and Natural Sciences" at the Taras Shevchenko National University of Kyiv. A.Z. acknowledges the partial support of the EU Horizon 2020 Research and Innovation Staff Exchange Program (RISE) under the Marie Skłodowska-Curie Action (project "UNAT", no. 101008159) and the French Ministry of Education and the EU, The Programme for the Emergency Reception of Scientists in Exile, the "PAUSE" Program.

## REFERENCES

(1) Wang, T.; Zang, X.; Wang, X.; Gu, X.; Shao, Q.; Cao, N. Recent advances in fluorine-doped/fluorinated carbon-based materials for supercapacitors. *Energy Storage Mater.* **2020**, *30*, 367−384.
(2) Jung, M.-J.; Jeong, E.; Lee, Y.-S. The surface chemical properties of multi-walled carbon nanotubes modified by thermal fluorination for electric double-layer capacitor. *Appl. Surf. Sci.* **2015**, *347*, 250−257.
(3) Groult, H.; Nakajima, T.; Perrigaud, L.; Ohzawa, Y.; Yashiro, H.; Komaba, S.; Kumagai, N. Surface-fluorinated graphite anode materials for Li-ion batteries. *J. Fluorine Chem.* **2005**, *126*, 1111−1116.
(4) Zaderko, A. N.; Grishchenko, L. M.; Pontiroli, D.; Scaravonati, S.; Riccò, M.; Diyuk, V. E.; Skryshevsky, V. A.; Lisnyak, V. V. Enhancing the performance of carbon electrodes in supercapacitors through medium-temperature fluoroalkylation. *Appl. Nanosci.* **2022**, *12*, 361−376.
(5) Kim, M. H.; Yang, J. H.; Kang, Y. M.; Park, S. M.; Han, J. T.; Kim, K. B.; Roh, K. C. Fluorinated activated carbon with superb kinetics for the supercapacitor application in nonaqueous electrolyte. *Colloids Surf., A* **2014**, *443*, 535−539.
(6) Velasco, L. F.; Kim, K. H.; Lee, Y.-S.; Lodewyckx, P. Influence of fluorine doping of activated carbon fibers on their water vapor adsorption characteristics. *Front. Chem.* **2021**, *8*, 593756.
(7) Sugiyama, H.; Hattori, Y. Selective and enhanced $CO_2$ adsorption on fluorinated activated carbon fibers. *Chem. Phys. Lett.* **2020**, *758*, 137909.
(8) Tressaud, A.; Boltalina, O. V.; Nakajima, T. *New Fluorinated Carbons: Fundamentals and Applications*, 1 ed.; Academic Press: Amsterdam, The Netherlands, 2016.
(9) Meng, L. Y.; Park, S.-J. Superhydrophobic carbon-based materials: A review of synthesis, structure, and applications. *Carbon Lett.* **2014**, *15*, 89−104.
(10) Watanabe, N.; Nakajima, T.; Touhara, H. *Graphite Fluorides*; Elsevier: Amsterdam, The Netherlands, 2013.
(11) Feng, W.; Long, P.; Feng, Y.; Li, Y. Two-Dimensional Fluorinated Graphene: Synthesis, Structures, Properties and Applications. *Adv. Sci.* **2016**, *3*, 1500413.
(12) Inagaki, M.; Kang, F. Graphene derivatives: graphane, fluorographene, graphene oxide, graphyne and graphdiyne. *J. Mater. Chem. A* **2014**, *2*, 13193−13206.
(13) Adamska, M.; Narkiewicz, U. Fluorination of Carbon Nanotubes − A Review. *J. Fluorine Chem.* **2017**, *200*, 179−189.
(14) Liu, Y.; Vander Wal, R. L.; Khabashesku, V. N. Functionalization of Carbon Nano-onions by Direct Fluorination. *Chem. Mater.* **2007**, *19*, 778−786.
(15) Struzzi, C.; Scardamaglia, M.; Colomer, J.-F.; Verdini, A.; Floreano, L.; Snyders, R.; Bittencourt, C. Fluorination of vertically aligned carbon nanotubes: from $CF_4$ plasma chemistry to surface functionalization. *Beilstein J. Nanotechnol.* **2017**, *8*, 1723−1733.
(16) Lee, C.; Han, Y.-J.; Seo, Y. D.; Nakabayashi, K.; Miyawaki, J.; Santamaría, R.; Menéndez, R.; Yoon, S. H.; Jang, J. $C_4F_8$ plasma treatment as an effective route for improving rate performance of natural/synthetic graphite anodes in lithium ion batteries. *Carbon* **2016**, *103*, 28−35.
(17) Kang, J. H.; Takhar, D.; Kuznetsov, O. V.; Khabashesku, V. N.; Kelly, K. F. Fluorination and defluorination of carbon nanotubes: A nanoscale perspective. *Chem. Phys. Lett.* **2012**, *534*, 43−47.
(18) Sato, Y.; Itoh, K.; Hagiwara, R.; Fukunaga, T.; Ito, Y. On the So-Called "Semi-Ionic" C−F Bond Character in Fluorine−GIC. *Carbon* **2004**, *42*, 3243−3249.
(19) Shi, J.; Fan, M.; Qiao, J.; Liu, Y. Nitrogen and chlorine dual-doped mesoporous carbon as efficient non-precious electrocatalyst for oxygen reduction reaction both in alkaline and acidic electrolytes. *Chem. Lett.* **2014**, *43*, 1484−1486.
(20) Miao, S.; Xu, J.; Tang, D.; Zhang, W.; Wang, Y.; Huang, Y.; Wang, J.; Zhao, Z.; Xin, S. N. S Dual Doped Mesoporous Carbon Supported $Co_9S_8$ Nanoparticles as Efficient Hydrogen Evolving Electrocatalysts in a Wide pH Range. *ChemistrySelect* **2021**, *6*, 9513−9516.
(21) Emran, M. Y.; Shenashen, M. A.; Eid, A. I.; Selim, M. M.; El-Safty, S. A. Portable sensitive and selective biosensing assay of dopamine in live cells using dual phosphorus and nitrogen doped carbon urchin-like structure. *Chem. Eng. J.* **2022**, *430*, 132818.
(22) Liang, C.; Xie, X.; Shi, Q.; Feng, J.; Zhang, D.; Huang, X. Nitrogen/sulfur-doped dual-emission carbon dots with tunable fluorescence for ratiometric sensing of ferric ions and cell membrane imaging. *Appl. Surf. Sci.* **2022**, *572*, 151447.
(23) Mirhosseyni, M. S.; Nemati, F. Metal-free aerobic oxidation of benzyl alcohols over the selective N, P dual-doped hollow carbon sphere as the efficient and sustainable heterogeneous catalyst under mild reaction condition. *Microporous Mesoporous Mater.* **2022**, *329*, 111514.
(24) Wan, H.; Shen, X.; Jiang, H.; Zhang, C.; Jiang, K.; Chen, T.; Shi, L.; Dong, L.; He, C.; Xu, Y.; Li, J.; Chen, Y. Biomass-derived N/S dual-doped porous hard-carbon as high-capacity anodes for lithium/sodium ions batteries. *Energy* **2021**, *231*, 121102.
(25) Tiwari, B.; Joshi, A.; Munjal, M.; Kaur, G.; Sharma, R. K.; Singh, G. Synergistic combination of N/P dual-doped activated carbon with redox-active electrolyte for high performance supercapacitors. *J. Phys. Chem. Solids* **2022**, *161*, 110449.
(26) Diyuk, V. E.; Zaderko, A. N.; Grishchenko, L. M.; Afonin, S.; Mariychuk, R.; Boldyrieva, O. Yu.; Skryshevsky, V. A.; Kaňuchová, M.; Lisnyak, V. V. Surface chemistry of fluoroalkylated nanoporous activated carbons: XPS and $^{19}F$ NMR study. *Appl. Nanosci.* **2022**, *12*, 637−650.
(27) Diyuk, V. E.; Zaderko, A. N.; Grishchenko, L. M.; Afonin, S.; Mariychuk, R.; Kaňuchová, M.; Lisnyak, V. V. Preparation, texture and surface chemistry characterization of nanoporous-activated carbons co-doped with fluorine and chlorine. *Appl. Nanosci.* **2022**, *12*, 2103−2116.
(28) Zhong, Z.; Huang, Y.; Yang, W. A simple photochemical method for surface fluorination using perfluoroketones. *Chin. Chem. Lett.* **2024**, *35*, 109339.
(29) Dmowski, W. 1,2-Dibromotetrafluoroethane (Freon 114B2) as a building block for fluorine compounds. *J. Fluorine Chem.* **2012**, *142*, 6−13.
(30) UNEP. *Handbook for the Montreal Protocol on Substances that Deplete the Ozone Layer*, 13th ed.; Ozone Secretariat: Nairobi, Kenya, 2019.
(31) de Boer, J.; Harrad, S.; Sharkey, M. The European Regulatory Strategy for flame retardants − The right direction but still a risk of getting lost. *Chemosphere* **2024**, *347*, 140638.
(32) Ma, C.; Kumagai, S.; Saito, Y.; Yoshioka, T.; Huang, X.; Shao, Y.; Ran, J.; Sun, L. Recent Advancements in Pyrolysis of Halogen-Containing Plastics for Resource Recovery and Halogen Upcycling: A State-of-the-Art Review. *Environ. Sci. Technol.* **2024**, *58*, 1423−1440.
(33) Yang, X.; Sun, L.; Xiang, J.; Hu, S.; Su, S. Pyrolysis and dehalogenation of plastics from waste electrical and electronic equipment (WEEE): a review. *Waste Manage.* **2013**, *33*, 462−473.
(34) Vehlow, J.; Bergfeldt, B.; Hunsinger, H.; Jay, K.; Mark, F. E.; Tange, L.; Drohmann, D.; Fisch, H. Recycling of bromine from plastics containing brominated flame retardants in state of the-art combustion facilities; European Brominated Flame Retardant


https://doi.org/10.1021/acsomega.4c04179
*ACS Omega* 2024, 9, 38618−38628

Industry Panel: Brussels, Belgium, 2002. http://www.ebfrip.org/download/tamara.pdf (accessed April 21, 2024).
(35) Dwivedi, N.; Yeo, R. J.; Satyanarayana, N.; Kundu, S.; Tripathy, S. K.; Bhatia, C. S. Understanding the Role of Nitrogen in Plasma-Assisted Surface Modification of Magnetic Recording Media with and without Ultrathin Carbon Overcoats. *Sci. Rep.* **2015**, *5*, 7772.
(36) Gengenbach, T. R.; Major, G. H.; Linford, M. R.; Easton, C. D. Practical guides for X-ray photoelectron spectroscopy (XPS): Interpreting the carbon 1s spectrum. *J. Vac. Sci. Technol., A* **2021**, *39*, 013204.
(37) Chen, X.; Wang, X.; Fang, D. A review on C 1s XPS spectra for some kinds of carbon materials. *Fullerenes, Nanotub. Carbon Nanostruct.* **2020**, *28*, 1048−1058.
(38) Ferraria, A. M.; Lopes da Silva, J. D.; Botelho do Rego, A. M. XPS Studies of Directly Fluorinated HDPE: Problems and Solutions. *Polymer* **2003**, *44* (23), 7241−7249.
(39) Dai, Y.; Cai, S.; Wu, L.; Yang, W.; Xie, J.; Wen, W.; Zheng, J.-C.; Zhu, Y. Surface Modified $CF_x$ Cathode Material for Ultrafast Discharge and High Energy Density. *J. Mater. Chem. A* **2014**, *2* (48), 20896−20901.
(40) Guerin, K.; Dubois, M.; Houdayer, A.; Hamwi, A. Applicative performances of fluorinated carbons through fluorination routes: A review. *J. Fluorine Chem.* **2012**, *134*, 11−17.
(41) Zhou, S.; Sherpa, S. D.; Hess, D. W.; Bongiorno, A. Chemical Bonding of Partially Fluorinated Graphene. *J. Phys. Chem. C* **2014**, *118*, 26402−26408.
(42) Forster-Tonigold, K.; Buchner, F.; Bansmann, J.; Behm, R. J.; Groß, A. A Combined XPS and Computational Study of the Chemical Reduction of BMP-TFSI by Lithium. *Batteries Supercaps* **2022**, *5*, No. e202200307.
(43) Liu, Y.; Jiang, L.; Wang, H.; Wang, H.; Jiao, W.; Chen, G.; Zhang, P.; Hui, D.; Jian, X. A brief review for fluorinated carbon: synthesis, properties and applications. *Nanotechnol. Rev.* **2019**, *8*, 573−586.
(44) Feng, W. Status and development trends for fluorinated carbon in China. *New Carbon Mater.* **2023**, *38*, 130−142.
(45) Wang, B.; Wang, J.; Zhu, J. Fluorination of Graphene: A Spectroscopic and Microscopic Study. *ACS Nano* **2014**, *8*, 1862−1870.
(46) Dolbier, W. R., Jr. *Guide to Fluorine NMR for Organic Chemists*, 2nd ed.; Wiley, Hoboken, NJ, USA, 2016; pp 239−240.
(47) Parmentier, J.; Schlienger, S.; Dubois, M.; Disa, E.; Masin, F.; Centeno, T. A. Structural/textural properties and water reactivity of fluorinated activated carbons. *Carbon* **2012**, *50*, 5135−5147.
(48) Hagaman, E. W.; Murray, D. K.; Del Cul, G. D. Solid State $^{13}C$ and $^{19}F$ NMR Characterization of Fluorinated Charcoal. *Energy Fuels* **1998**, *12*, 399−408.
(49) Panich, A. M. Nuclear magnetic resonance study of fluorine-graphite intercalation compounds and graphite fluorides. *Synth. Met.* **1999**, *100*, 169−185.
(50) Vyalikh, A.; Bulusheva, L. G.; Chekhova, G. N.; Pinakov, D. V.; Okotrub, A. V.; Scheler, U. Fluorine patterning in room-temperature fluorinated graphite determined by solid-state NMR and DFT. *J. Phys. Chem. C* **2013**, *117*, 7940−7948.
(51) Moldoveanu, S. C. *Pyrolysis of Organic Molecules with Applications to Health and Environmental Issues Techniques and Instrumentation in Analytical Chemistry*; Elsevier: New York, NY, USA, 2010; Vol. *28*, p 724.
(52) Multian, V.; Kinzerskyi, F.; Vakaliuk, A.; Grishchenko, L. M.; Diyuk, V. E.; Boldyrieva, O. Y.; Kozhanov, V. O.; Mischanchuk, O. V.; Lisnyak, V. V.; Gayvoronsky, V. Y. Surface Response of Brominated Carbon Media on Laser and Thermal Excitation: Optical and Thermal Analysis Study. *Nanoscale Res. Lett.* **2017**, *12*, 146.
(53) Shen, W.; Li, Z.; Liu, Y. Surface chemical functional groups modification of porous carbon. *Recent Pat. Chem. Eng.* **2008**, *1*, 27−40.
(54) Diyuk, V. E.; Zaderko, A. N.; Veselovska, K. I.; Lisnyak, V. V. Functionalization of surface of carbon materials with bromine vapors at mediate high temperature: a thermogravimetric study. *J. Therm. Anal. Calorim.* **2015**, *120*, 1665−1678.
(55) Rocha, R. P.; Pereira, M. F. R.; Figueiredo, J. L. Characterisation of the surface chemistry of carbon materials by temperature-programmed desorption: An assessment. *Catal. Today* **2023**, *418*, 114136.
(56) Liu, L.; Zeng, Y.; Tan, S. J.; Xu, H.; Do, D. D.; Nicholson, D.; Liu, J. On the mechanism of water adsorption in carbon micropores − A molecular simulation study. *Chem. Eng. J.* **2019**, *357*, 358−366.
(57) Lewis, R. J. *Sax's Dangerous Properties of Industrial Materials*, 9th ed.; Van Nostrand Reinhold: New York, NY, USA, 1996; Vol. *1*−*3*, p 1699.
(58) Figueiredo, J. L.; Pereira, M. F. R.; Freitas, M. M. A.; Orfao, J. J. M. Modification of the surface chemistry of activated carbons. *Carbon* **1999**, *37*, 1379−1389.
(59) Plugge, M.; Tapscott, R. E.; Beeson, H. D.; Zallen, D.; Walker, J. L.; Campbell, P. *Fire Suppression by HALON 2402*; Naval Air Systems, Command Department of Navy: Washington, DC, USA, 1987; Vol. *I*, pp 131−132.
(60) Tabrizi, F. F.; Dunker, M.; Hiller, A.; Beckmann, M. Maximizing $HBr/Br_2$ in the flue gas and prevention of secondary pollution during the oxy-combustion of brominated waste electrical and electronic equipment part 1- thermodynamic considerations. *Environ. Pollut.* **2020**, *263*, 114410.
(61) Lu, Y.; Zhang, T.; Lily, M.; Wang, W.; Liu, F.; Wang, W. The catalytic effects of $H_2O$, basic and acidic catalysts on the gas-phase hydrolysis mechanism of carbonyl fluoride ($CF_2O$). *Int. J. Quantum Chem.* **2021**, *121*, No. e26657.
(62) Menéndez, J. A.; Phillips, J.; Xia, B.; Radovic, L. R. On the modification and characterization of chemical surface properties of activated carbon: In the search of carbons with stable basic properties. *Langmuir* **1996**, *12*, 4404−4410.


https://doi.org/10.1021/acsomega.4c04179
*ACS Omega* 2024, 9, 38618−38628